Tunable Resonant and Nonresonant Interactions between a Phase Qubit and *LC* Resonator

M. S. Allman, J. D. Whittaker, M. Castellanos-Beltran, K. Cicak, F. da Silva, M. P. DeFeo, F. Lecocq, A. Sirois, J. D. Teufel, J. Aumentado, and R. W. Simmonds[*]

National Institute of Standards and Technology, 325 Broadway Street, Boulder, Colorado 80305-3328, USA

We use a flux-biased radio frequency superconducting quantum interference device (rf SQUID) with an embedded flux-biased direct current SQUID to generate strong resonant and nonresonant tunable interactions between a phase qubit and a lumped-element resonator. The rf SQUID creates a tunable magnetic susceptibility between the qubit and resonator providing resonant coupling strengths from zero to near the ultrastrong coupling regime. By modulating the magnetic susceptibility, nonresonant parametric coupling achieves rates > 100 MHz. Nonlinearity of the magnetic susceptibility also leads to parametric coupling at the subharmonics of the qubit-resonator detuning.

The need to develop robust schemes for controlling qubit-qubit and qubit-cavity bus interactions is generic to all physical approaches for implementing a large scale quantum information processor or quantum simulators [1,2]. With superconducting circuits [3], the most widely used method of controllable coupling is with tunable qubits or cavities and with passive, static, "always-on" capacitive coupling [3–6]. Interaction strengths are then controlled through the adjustable size of frequency detunings between the different resonant elements [6–10]. Although very simple and convenient for a small number of elements, the ability to provide sufficient detuning between all coupled elements becomes impractical when scaling to large numbers of qubits or cavities [11]. Additionally, it is difficult to selectively tune individual elements fast enough to avoid unwanted interactions from inevitably crossing resonant frequencies of spectator elements. Finally, simultaneously engineering an optimal performance and strong resonance conditions can be challenging [12–14].

One major advantage with superconducting circuit approaches is their ability to use Josephson junctions as flux-tunable inductors, not only for tunable qubits and cavities, but also for individual, tunable coupling elements [11–22]. Experimental demonstrations began in the classical regime [18,20,22], while quantum implementations [21,23–27] have still relied on resonant interactions, without addressing the problem of optimal operating points. Other theoretical proposals [28–33] and experiments [34–38] have introduced parametric interactions between nonresonant elements to solve this problem. Here the nonlinearity is provided by the qubits and includes some amount of always-on coupling. Further theoretical proposals have provided a unique solution to all the major problems discussed above, by providing parametric interactions through individual tunable coupling elements [12,39–42]. Early successful experiments were performed,

but suffered from difficulties associated with fully integrating the coupler into both the qubits and their readout [13,14]. Here, we discuss the use of an individual, stand-alone rf superconducting quantum interference device (SQUID)-type coupling element [15,18,20,22,24] that introduces negligible energy loss (see Supplemental Material, part V [43]) and requires minimal or no modification to the qubit or cavity architecture. We have made three major advances in this Letter: (1) resonant coupling can be performed with rates ranging from zero to near ultrastrong values close to 10% of the resonant frequency, (2) nonresonant parametric coupling can be performed with rates > 100 MHz with an architecture that allows for the cancellation of static coupling, and (3) we have demonstrated a new multiphoton parametric coupling mechanism. All of the behavior observed agrees with theoretical predictions.

Shown in Fig. 1, our circuit design consists of a phase qubit with geometric inductance L_q, critical current I_{q0}, and shunt capacitance C_q, which is inductively coupled to a rf SQUID loop through a mutual inductance M_{qc}. The rf SQUID loop acts as a tunable coupler with geometric inductance L_c, and two junctions, with critical currents, I_{c01} and I_{c02}, that form a dc SQUID that can modify the rf SQUID's properties. The geometric inductance of the dc SQUID is small enough to neglect in the following theoretical analysis. The rf SQUID is inductively coupled to a lumped-element resonator through a mutual inductance M_{cr}. The resonator has a geometric inductance L_r, capacitance C_r, and resonant frequency ω_r. The phase qubit [44] is controlled by a single flux-bias line that provides both dc and rf flux, $\varphi_q = \Phi_q/\Phi_0$ (Φ_0 is the magnetic flux quantum). Qubit measurement is performed using a short (≈ 5 ns) pulse that induces tunneling of the $|e\rangle$ state with probability P_e, without appreciable tunneling of the $|g\rangle$ state [7]. The coupler is controlled by two external flux-bias
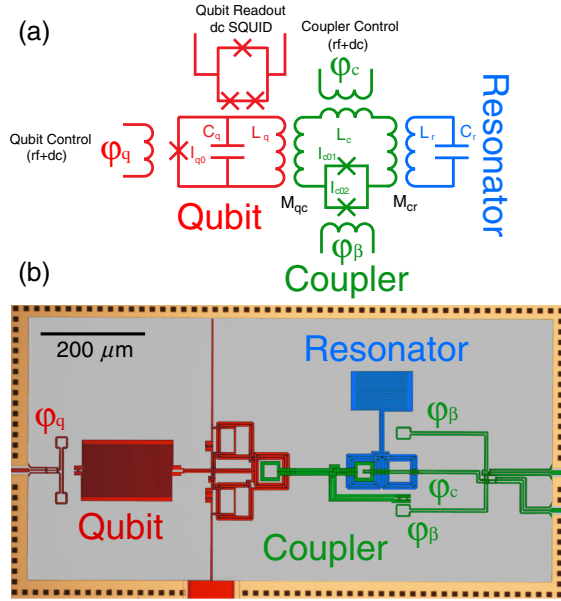
FIG. 1 (color online). (a) Circuit diagram for the phase qubit, coupler, and resonator. The qubit's design parameters are $L_q \approx 2$ nH, $I_{q0} \approx 0.5$ μA, $C_q \approx 0.5$ pF, and $M_{qc} \approx 70$ pH. The coupler's design parameters are $L_c \approx 300$ pH, $I_{c01} = I_{c02} \approx 0.5$ μA. The resonator's design parameters are $L_r \approx 1.8$ nH, $C_r \approx 0.26$ pF, and $M_{cr} \approx 85$ pH. All mutual inductances to flux-bias lines were designed to be ≈ 2 pH.(b) Colorized optical micrograph of the device. All flux biases $\varphi_i = \Phi_i/\Phi_o$ are normalized by the magnetic flux quantum, $\Phi_o = h/2e$.

lines. One line applies flux $\varphi_c = \Phi_c/\Phi_0$ to the rf SQUID loop, while the other line applies flux, $\varphi_\beta = \Phi_\beta/\Phi_0$, to the embedded dc SQUID. The chip is mounted in a shielded box onto the mixing chamber of a cryogen-free dilution refrigerator with a base temperature $T = 11$ mK.

The critical current I_{c0} of the embedded dc SQUID can be tuned by varying φ_β [45]. The functional form is

$$I_{c0}(\varphi_\beta) = \sqrt{I_+^2 \cos^2\frac{\varphi_\beta}{2} + I_-^2 \sin^2\frac{\varphi_\beta}{2}}, \qquad (1)$$

where $I_\pm = I_{01} \pm I_{02}$ is the sum and difference of the individual critical currents of the junctions comprising the dc SQUID. The circulating dc screening current in the rf SQUID is given by

$$i_c = -\sin[2\pi\varphi_{xc} + \beta(\varphi_\beta)i_c], \qquad (2)$$

where $i_c = I_c/I_{c0}(\varphi_\beta)$ is the normalized circulating coupler current, $\varphi_{xc} = (\varphi_c + M_{qc}I_q/\Phi_0)$ is the net external flux applied to the coupler, I_q is the circulating current in the qubit inductor, and $\beta(\varphi_\beta) = 2\pi L_c I_{c0}(\varphi_\beta)/\Phi_0$. Here $\beta(\varphi_\beta) < 1$ so that the coupler circulating current is single valued [24,25]. The coupler circulating current generates an effective mutual inductance between the qubit and resonator that is a function of both φ_{xc} and φ_β, given by

$$M_{\mathrm{eff}}(\varphi_{xc}, \varphi_\beta) = M_0\chi(\varphi_{xc}, \varphi_\beta), \qquad (3)$$

where $M_0 = M_{qc}M_{cr}/L_c$ and $\chi(\varphi_{xc}, \varphi_\beta)$ is a linear, first-order magnetic susceptibility between the qubit and resonator, given by

$$\chi(\varphi_{xc}, \varphi_\beta) = \frac{L_c I_{c0}}{\Phi_0}\frac{\partial i_c}{\partial\varphi_{xc}}. \qquad (4)$$

The effective mutual inductance implies a coupling between the qubit and resonator given by

$$g(\varphi_{xc}, \varphi_\beta) = g_0\chi(\varphi_{xc}, \varphi_\beta) + g_{\mathrm{res}}, \qquad (5)$$

where $g_0 = (\omega_{q0}/2)M_0/\sqrt{L_q L_r}$ [42], $\omega_{q0} = 1/\sqrt{L_q C_q}$, and g_{res} is any residual direct coupling between the qubit and the resonator from either capacitive, inductive, or higher-order virtual-photon processes that access the coupler's own high frequency resonant modes [25,41]. When $\varphi_{xc} = n/2$, for integer n, the linear susceptibility takes on the following φ_β-dependent extrema:

$$\chi_{\max}(\varphi_\beta) = \frac{\beta(\varphi_\beta)}{1 - \beta(\varphi_\beta)} \quad \text{for } n_{\mathrm{odd}}, \qquad (6)$$

$$\chi_{\min}(\varphi_\beta) = -\frac{\beta(\varphi_\beta)}{1 + \beta(\varphi_\beta)} \quad \text{for } n_{\mathrm{even}}. \qquad (7)$$

We note some interesting features; $\chi_{\max}(\varphi_\beta)$ increases without bound as $\beta(\varphi_\beta)$ is tuned towards unity and $\chi(\varphi_{xc}, \varphi_\beta)$ can be both positive and negative (an additional "twist" in the coupler loop can also reverse its sign [26]). This second feature provides a built-in mechanism to engineer the cancellation of any residual direct coupling g_{res} regardless of its sign [25,26]. This is not only important to ensure the resonant coupling strength can be tuned to $g = 0$, resulting in a large "on/off ratio," but also for engineering optimal performance for nonresonant interactions, as discussed below.

Near resonance, the interactions between the qubit and resonator are governed by the well-known Jaynes-Cummings model [7]. In the rotating frame of the uncoupled qubit and resonator, the interaction Hamiltonian is

$$H_I = \hbar g(\varphi_{xc}, \varphi_\beta)[e^{i\Delta t}\sigma^- a^\dagger + e^{-i\Delta t}\sigma^+ a], \qquad (8)$$

where $\Delta = \omega_{ge} - \omega_r$ is the detuning of the qubit and resonator, $\omega_{ge} = (E_e - E_g)/\hbar$, and ω_r is the resonator frequency. When the detuning becomes large relative to g, the time-dependent exponentials rotate rapidly, resulting in negligible interactions. For nonresonant interactions, if g is harmonically modulated in time at Δ to counter the exponentials, the interaction terms once again become stationary. This is the essence of parametric coupling. Physically, "pump photons" at frequency Δ, introduced into

the system via the coupler, make up the energy difference between the qubit and resonator, allowing them to exchange energy. Next, we show that the nonlinearity of the coupling curve $g_0\chi(\varphi_{xc},\varphi_\beta)$ can also lead to a new parametric coupling condition at the subharmonics of Δ.

The coupling strength g is modified by modulating φ_{xc} through the coupler bias,

$$\varphi_c(t) = \varphi_{dc} + \delta\varphi_c \cos\omega_p t, \quad (9)$$

where φ_{dc} is a dc flux offset that sets the resonant coupling strength and $\delta\varphi_c$ is the amplitude of the rf modulation. For $\delta\varphi_c \ll 1$, $g(t)$ can be found by Taylor expanding Eq. (5) in φ_{xc} to get

$$g(t) = g_0 \sum_{n=0}^{\infty} \chi_{\varphi_{dc}}^{(n)} \delta\varphi_{xc}^n \frac{(e^{i\omega_p t} + e^{-i\omega_p t})^n}{n!2^n}, \quad (10)$$

where $\chi_{\varphi_{dc}}^{(n)}$ is the nth derivative of $\chi(\varphi_{xc},\varphi_\beta)$ with respect to φ_{xc}, evaluated at $\varphi_{xc} = \varphi_{dc}$. Note that $\chi_{\varphi_{dc}}^{(n)}$ is a function of φ_β. Equation (10) implies that multiphoton parametric interactions are predicted at pump frequencies such that $n\omega_p = \Delta$. The lowest-order n-photon interaction is (discarding counterrotating terms)

$$H_I^{(n)} = \hbar \frac{g_0\chi_{\varphi_{dc}}^{(n)}\delta\varphi_{xc}^n}{n!2^n}[\sigma^- a^\dagger + \sigma^+ a]. \quad (11)$$

The higher-order terms lead to saturation of the coupl.ing strength when the pump amplitude becomes large. From Eq. (11), we see that the overall coupling strength in the n-photon parametric case is governed by both $\delta\varphi_{xc}$ and the derivative $\chi_{\varphi_{dc}}^{(n)}$. Figure 2(a) shows a plot of $\chi(\varphi_{xc},\varphi_\beta)$ for various $\beta(\varphi_\beta)$. As mentioned, $\chi_{\max}(\varphi_\beta)$ increases with increasing $\beta(\varphi_\beta)$, but $\chi_{\varphi_{dc}}^{(n)}$ also considerably increases with $\beta(\varphi_\beta)$ at operating points near $\varphi_{xc} = \pm 0.5$. Notice that through careful design, it should be possible to engineer g_{res} in such a way to offset the static coupling curve $g(\varphi_{xc},\varphi_\beta)$, so that zero static coupling occurs near $\varphi_{xc} = \pm 0.5$, where $\chi_{\varphi_{dc}}^{(n)} \gg 1$. Operating here ensures $g = 0$ when the pump is off, allowing an extremely large on/off ratio for nonresonant interactions, even for small Δ's (see Supplemental Material, part IV [43]). In the experimental results described below, we did not perform this further optimization, but chose to investigate the largest possible coupling strengths with our existing circuit.

First, we measure the coupler's circulating current I_c as a function of φ_{xc} (as described in Ref. [25] and Supplemental Material, part II [43]) for various $\beta(\varphi_\beta)$. Next, we experimentally map out $\chi(\varphi_{xc},\varphi_\beta)$ by measuring resonant coupling rates $2g$ as a function of φ_{xc} and φ_β. This is achieved through spectroscopically observing the splitting of the coupled qubit and resonator modes [25]. The
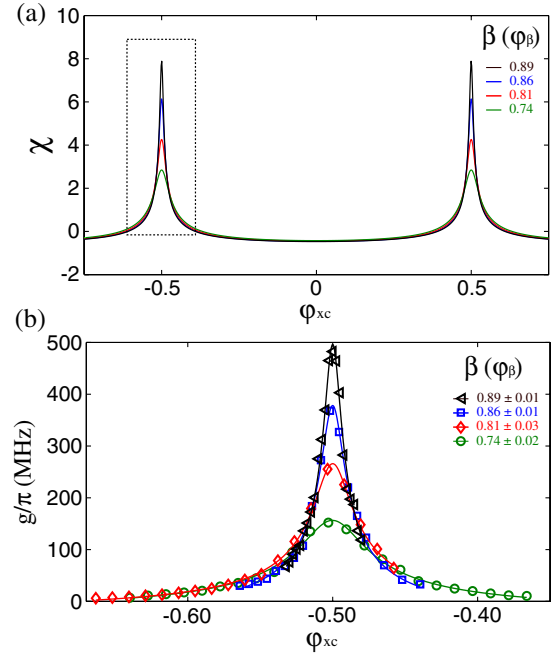

FIG. 2 (color online). (a) Theoretical plot of the magnetic susceptibility χ as a function of φ_{xc} for $\beta(\varphi_\beta) = 0.74, 0.81, 0.86, 0.89$, corresponding to the measurements of resonant coupling rates plotted in (b). Derivatives of χ increase sharply near $\varphi_{xc} = \pm 0.5$ as $\beta(\varphi_\beta)$ approaches unity, allowing stronger parametric coupling with increasing $\beta(\varphi_\beta)$. (b) Resonant coupling rates along with theoretical fits.

resonator's frequency is $\omega_r/2\pi \approx 7.2$ GHz and modulates slightly with φ_{xc} as discussed in [25]. Several spectroscopies are taken as a function of φ_{xc} to map out coupling rates for the fixed rf SQUID critical current. The critical current is then modified by changing φ_β and the whole process is repeated. Figure 2(b) is a plot of measured resonant coupling rates as a function of φ_{xc} for different rf SQUID critical currents. The maximum coupling rate shown is $2g/2\pi = 482$ MHz, approaching the ultrastrong coupling regime, with $2g/\omega_r \approx 7\%$ [46–48]. Mode splittings with $2g/2\pi > 500$ MHz were also observed with this device, but due to the resonator's close proximity to the qubit's minimum operating frequency, the data were difficult to fit reliably. A device designed with a higher resonator frequency would allow more quantitative measurements in the ultrastrong coupling regime. Without performing an exhaustive search, the minimum resonant coupling rate measured with this device was $2g_{\min}/2\pi = 6$ MHz, still visible within the qubit linewidth of about 7 MHz, providing a lower bound for the on/off ratio of approximately 80. We determined $2g_{\mathrm{res}}/2\pi \approx 10$ MHz and $2g_0\chi_{\min}/2\pi \approx -25$ MHz, ensuring that the coupling strength passes through zero, as seen in similar devices [25] (see Supplemental Material, part III [43]).

Once the resonant coupling curves are measured, nonresonant parametric interactions can be probed by setting the coupler to an operating point where the modulation in g
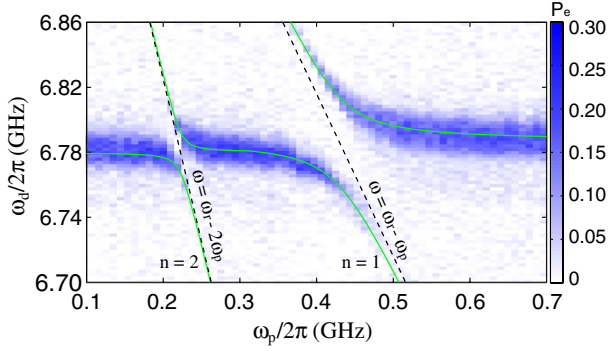
FIG. 3 (color online).   Qubit spectroscopy data with rf pump power at frequency ω_p applied to φ_c along with a theoretical fit including the $n = 1$ and $n = 2$ photon mode splittings.

with φ_{xc} is appreciable [see Fig. 2(b)]. The qubit is detuned from the resonator by an amount Δ and a pump tone of amplitude $\delta\varphi_c$ and frequency ω_p is applied to φ_c in addition to the dc offset. The frequency of the pump tone is swept. Qubit spectroscopy is then measured as a function of ω_p and $\delta\varphi_{xc} = \delta\varphi_c$. For a given $\delta\varphi_{xc}$, mode splitting is observed when $\omega_p = \Delta$, indicating parametric interactions between the qubit and the resonator. Figure 3 shows a typical case. The qubit and resonator are detuned by $\Delta/2\pi = 429$ MHz. The coupler is biased with dc flux offsets, $\varphi_{xc} = -0.527$ and $\beta(\varphi_\beta) = 0.81$, corresponding to the red curve in Fig. 2(b). The applied pump power to the coupler coil is -58 dBm. Notice that we also find mode splitting at subharmonics, $\omega_p = \Delta/2$. This is the result of the n-photon process described above, where $n = 2$ photons at half the detuning frequency are upconverted to a single resonant pump photon. Depending on the operating conditions, $n = 3$ and $n = 4$ photon events were also observed with this sample, but were too small to present quantitatively (see Supplemental Material, part VI [43] for an example). Included in Fig. 3 are theory fits of the coupled-mode frequencies along with asymptotes that obey the linear relation $\omega = \omega_r - n\omega_p$, where ω_r is the resonator frequency, ω_p is the pump frequency, and n is number of photons absorbed.

In Fig. 4, we plot the resulting mode splittings from the $n = 1$ and $n = 2$ photon processes for $\beta(\varphi_\beta) = 0.81$ (red curves) and $\beta(\varphi_\beta) = 0.86$ (blue curves). For each $\beta(\varphi_\beta)$, we increase the pump power to investigate the power dependence of the splittings. For the theoretical predictions, we use only the lowest-order terms from the expansion of Eq. (10), the slopes $\chi^{(1)}_{\varphi_{dc}}$ and $\chi^{(2)}_{\varphi_{dc}}$ from numerically fitting the data shown in Fig. 2(b), and a single fit parameter for each curve $\delta\varphi_{xc}$ reported along with the corresponding drive powers in Fig. 4. To test the validity of these fits, we used a network analyzer to independently measure the available power at the input of the sample box in order to infer the expected rf flux applied to the rf SQUID loop. For example, when $\beta(\varphi_\beta) = 0.86$ and $\omega_p/2\pi = 429$ MHz, a
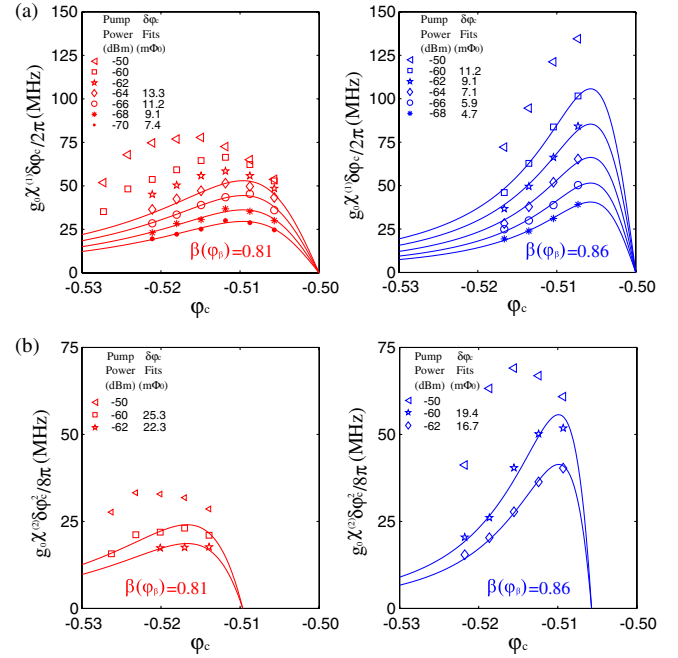

FIG. 4 (color online).   (a) $n = 1$ photon mode splittings corresponding to $\beta(\varphi_\beta) = 0.81$ (red curves) and $\beta(\varphi_\beta) = 0.86$ (blue curves) as a function of φ_{xc}. Data for pump powers ranging from -70 to -50 dBm are shown along with theoretical fits for the data below saturation. (b) $n = 2$ photon mode splittings for the same coupler settings in (a).

generator input power of -62 dBm provided a rf current $\delta I_b \approx 10$ μA to the bias coil. From the Φ_0 periodicity of the rf SQUID circulating current, we measured the mutual inductance between the bias coil and rf SQUID loop to be $M_{cb} = 1.72$ pH. Thus, the expected flux applied to the rf SQUID loop is $\delta\varphi_{xc}\Phi_0 = M_{cb}\delta I_b \approx 8.3$ mΦ_0, which agrees well with the corresponding fit value shown in Fig. 4(a). At lower powers, the lowest-order theory fits the data nicely. At higher powers, the coupling rate saturates, causing the data to significantly deviate from the lowest-order expansion term, as expected. The largest $n = 1$ parametric coupling rate observed was $2g/2\pi = 135$ MHz [shown in Fig. 4(a)]. For the parametric case, the on/off ratio can be limited by photon leakage through the pump's pulse gate, where 40 dB isolation leads to an on/off ratio of 100. In our case, we were mostly limited by a small Δ combined with a large static g at the chosen operating points, giving a maximum on/off ratio of 51. This can easily be increased by over an order of magnitude by increasing Δ, dynamically shifting the static coupling strength to $g = 0$, or through design improvements (see Supplemental Material, part IV [43]).

In summary, the rf SQUID coupler provides dynamic control over both resonant and nonresonant interactions. Both modes of operation rely on the dependence of the magnetic susceptibility between the qubit and resonator as a function of φ_{xc} and φ_β. By tuning the critical current of

the embedded dc SQUID, we control the maximum of the magnetic susceptibility, leading to resonant coupling rates approaching the ultrastrong coupling regime. The dependence of the magnetic susceptibility curve on φ_{xc} can be exploited to induce strong, nonresonant coupling by parametric modulation at the qubit-resonator difference frequency or subharmonics. Parametric coupling rates exceeding 100 MHz are possible. Future work will reduce dielectric losses, increase lifetimes, and explore parametric interactions at the sum frequency (or blue-sideband, familiar in trapped-ion systems), $\omega_p = \omega_{ge} + \omega_r$. This coupler is well suited for nonextended, nearest neighbor tunable coupling, generically important for constructing coupled-mode systems ubiquitous in physics, useful for both quantum information architectures and quantum simulators.

---

*simmonds@boulder.nist.gov

[1] S. Lloyd, Science **273**, 1073 (1996).

[2] I. Buluta and F. Nori, Science **326**, 108 (2009).

[3] M. H. Devoret and R. J. Schoelkopf, Science **339**, 1169 (2013).

[4] H. Paik, D. I. Schuster, L. S. Bishop, G. Kirchmair, G. Catelani, A. P. Sears, B. R. Johnson, M. J. Reagor, L. Frunzio, L. I. Glazman, S. M. Girvin, M. H. Devoret, and R. J. Schoelkopf, Phys. Rev. Lett. **107**, 240501 (2011).

[5] A. A. Houck, H. E. Tuereci, and J. Koch, Nat. Phys. **8**, 292 (2012).

[6] E. Lucero, R. Barends, Y. Chen, J. Kelly, M. Mariantoni, A. Megrant, P. O'Malley, D. Sank, A. Vainsencher, J. Wenner, T. White, Y. Yin, A. N. Cleland, and J. M. Martinis, Nat. Phys. **8**, 719 (2012).

[7] M. A. Sillanpää, J. I. Park, and R. W. Simmonds, Nature (London) **449**, 438 (2007).

[8] J. Majer, J. M. Chow, J. M. Gambetta, J. Koch, B. R. Johnson, J. A. Schreier, L. Frunzio, D. I. Schuster, A. A. Houck, A. Wallraff, A. Blais, M. H. Devoret, S. M. Girvin, and R. J. Schoelkopf, Nature (London) **449**, 443 (2007).

[9] M. Hofheinz, E. M. Weig, M. Ansmann, R. C. Bialczak, E. Lucero, M. Neeley, A. D. O'Connell, H. Wang, J. M. Martinis, and A. N. Cleland, Nature (London) **454**, 310 (2008).

[10] F. Altomare, J. I. Park, K. Cicak, M. A. Sillanpää, M. S. Allman, D. Li, A. Sirois, J. A. Strong, J. D. Whittaker, and R. W. Simmonds, Nat. Phys. **6**, 777 (2010).

[11] Y. Makhlin, G. Schon, and A. Shnirman, Nature (London) **398**, 305 (1999).

[12] A. O. Niskanen, Y. Nakamura, and J.-S. Tsai, Phys. Rev. B **73**, 094506 (2006).

[13] A. O. Niskanen, K. Harrabi, F. Yoshihara, Y. Nakamura, S. Lloyd, and J. S. Tsai, Science **316**, 723 (2007).

[14] K. Harrabi, F. Yoshihara, A. O. Niskanen, Y. Nakamura, and J. S. Tsai, Phys. Rev. B **79**, 020507 (2009).

[15] J. E. Mooij, T. P. Orlando, L. Levitov, L. Tian, C. H. van der Wal, and S. Lloyd, Science **285**, 1036 (1999).

[16] J. Q. You, J. S. Tsai, and F. Nori, Phys. Rev. B **68**, 024510 (2003).

[17] A. Blais, A. M. van den Brink, and A. M. Zagoskin, Phys. Rev. Lett. **90**, 127901 (2003).

[18] T. V. Filippov, S. K. Tolpygo, J. Männik, and J. E. Lukens, IEEE Trans. Appl. Supercond. **13**, 1005 (2003).

[19] M. D. Kim and J. Hong, Phys. Rev. B **70**, 184525 (2004).

[20] M. G. Castellano, F. Chiarello, R. Leoni, D. Simeone, G. Torrioli, C. Cosmelli, and P. Carelli, Appl. Phys. Lett. **86**, 152504 (2005).

[21] T. Hime, P. A. Reichardt, B. L. T. Plourde, T. L. Robertson, C. E. Wu, A. V. Ustinov, and J. Clarke, Science **314**, 1427 (2006).

[22] V. Zakosarenko, N. Bondarenko, S. H. W. van der Ploeg, A. Izmalkov, S. Linzen, J. Kunert, E. I. M. Grajcar, and H.-G. Meyer, Appl. Phys. Lett. **90**, 022501 (2007).

[23] S. H. W. van der Ploeg, A. Izmalkov, A. M. van den Brink, U. Hübner, M. Grajcar, E. Il'ichev, H.-G. Meyer, and A. M. Zagoskin, Phys. Rev. Lett. **98**, 057004 (2007).

[24] R. Harris, A. J. Berkley, M. W. Johnson, P. Bunyk, S. Govorkov, M. C. Thom, S. Uchaikin, A. B. Wilson, J. Chung, E. Holtham, J. D. Biamonte, A. Yu. Smirnov, M. H. S. Amin, and Alec Maassen van den Brink, Phys. Rev. Lett. **98**, 177001 (2007).

[25] M. S. Allman, F. Altomare, J. D. Whittaker, K. Cicak, D. Li, A. Sirois, J. Strong, J. D. Teufel, and R. W. Simmonds, Phys. Rev. Lett. **104**, 177004 (2010).

[26] R. C. Bialczak, M. Ansmann, M. Hofheinz, M. Lenander, E. Lucero, M. Neeley, A. D. O'Connell, D. Sank, H. Wang, M. Weides, J. Wenner, T. Yamamoto, A. N. Cleland, and J. M. Martinis, Phys. Rev. Lett. **106**, 060501 (2011).

[27] S. J. Srinivasan, A. J. Hoffman, J. M. Gambetta, and A. A. Houck, Phys. Rev. Lett. **106**, 083601 (2011).

[28] Yu-xi Liu, L. F. Wei, J. S. Tsai, and F. Nori, Phys. Rev. Lett. **96**, 067003 (2006).

[29] S. Ashhab, S. Matsuo, N. Hatakenaka, and F. Nori, Phys. Rev. B **74**, 184504 (2006).

[30] G. S. Paraoanu, Phys. Rev. B **74**, 140504 (2006).

[31] A. Blais, J. Gambetta, A. Wallraff, D. I. Schuster, S. M. Girvin, M. H. Devoret, and R. J. Schoelkopf, Phys. Rev. A **75**, 032329 (2007).

[32] Yu-xi Liu, L. F. Wei, J. R. Johansson, J. S. Tsai, and F. Nori, Phys. Rev. B **76**, 144518 (2007).

[33] C. Rigetti and M. Devoret, Phys. Rev. B **81**, 134507 (2010).

[34] P. J. Leek, S. Filipp, P. Maurer, M. Baur, R. Bianchetti, J. M. Fink, M. Göppl, L. Steffen, and A. Wallraff, Phys. Rev. B **79**, 180511 (2009).

[35] P. C. de Groot, J. Lisenfeld, R. N. Schouten, S. Ashhab, A. Lupascu, C. J. P. M. Harmans, and J. E. Mooij, Nat. Phys. **6**, 763 (2010).

[36] E. Zakka-Bajjani, F. Nguyen, M. Lee, L. R. Vale, R. Simmonds, and J. Aumentado, Nat. Phys. **7**, 599 (2011).

[37] J. M. Chow, A. D. Córcoles, J. M. Gambetta, C. Rigetti, B. R. Johnson, J. A. Smolin, J. R. Rozen, G. A. Keefe, M. B. Rothwell, M. B. Ketchen, and M. Steffen, Phys. Rev. Lett. **107**, 080502 (2011).

[38] J. D. Strand, M. Ware, F. Beaudoin, T. A. Ohki, B. R. Johnson, A. Blais, and B. L. T. Plourde, Phys. Rev. B **87,** 220505 (2013).

[39] P. Bertet, C. J. P. M. Harmans, and J. E. Mooij, Phys. Rev. B **73,** 064512 (2006).

[40] M. Grajcar, Yu-xi Liu, F. Nori, and A. M. Zagoskin, Phys. Rev. B **74,** 172505 (2006).

[41] S. Ashhab, A. O. Niskanen, K. Harrabi, Y. Nakamura, T. Picot, P. C. de Groot, C. J. P. M. Harmans, J. E. Mooij, and F. Nori, Phys. Rev. B **77,** 014510 (2008).

[42] L. Tian, M. S. Allman, and R. W. Simmonds, New J. Phys. **10,** 115001 (2008).

[43] See Supplemental Material at http://link.aps.org/supplemental/10.1103/PhysRevLett.112.123601 for additional experimental results and details describing this system.

[44] R. W. Simmonds, K. M. Lang, D. A. Hite, S. Nam, D. P. Pappas, and J. M. Martinis, Phys. Rev. Lett. **93,** 077003 (2004).

[45] T. Van Duzer, *Principles of Superconductive Devices and Circuits* (Prentice-Hall, Inc., Englewood Cliffs, NJ, 1999).

[46] J. Bourassa, J. M. Gambetta, A. A. Abdumalikov, O. Astafiev, Y. Nakamura, and A. Blais, Phys. Rev. A **80,** 032109 (2009).

[47] P. Forn-Diaz, J. Lisenfeld, D. Marcos, J. J. Garcia-Ripoll, E. Solano, C. J. P. M. Harmans, and J. E. Mooij, Phys. Rev. Lett. **105,** 237001 (2010).

[48] T. Niemczyk, F. Deppe, H. Huebl, E. P. Menzel, F. Hocke, M. J. Schwarz, J. J. Garcia-Ripoll, D. Zueco, T. Huemmer, E. Solano, A. Marx, and R. Gross, Nat. Phys. **6,** 772 (2010).